2013-2172

19th AIAA/CEAS Aeroacoustics Conference, 27 - 29 May 2013, Berlin, Germany

Efficient Mode-Matching Based on Closed Form Integrals of Pridmore-Brown Modes

M. Oppeneer* S.W. Rienstra† P. Sijtsma‡
NLR/TUE *TUE* *NLR*

A new mode matching method is developed for acoustic modes in axially sectioned lined ducts with parallel, but otherwise arbitrary mean flow. The method is evaluated in detail for a circularly symmetric configuration (where the mean flow only depends on the radial coordinate), with so-called Pridmore-Brown modes, satisfying the radial Pridmore-Brown equation.

Classically, the matching of the modal representations at the interfaces between the sections is based on continuity of pressure and velocity in combination with projection to a suitable but unrelated set of test functions by means of a standard integral inner-product.

The alternative we propose here uses essentially the same Pridmore-Brown modes but instead of the standard inner-product we apply a particular bilinear form that can be evaluated in closed form. Apart from numerical efficiency, this approach features also a higher accuracy because it avoids the inherently inaccurate numerical quadrature of oscillating functions.

The results are compared with results obtained by an implementation of the classical approach, and the agreement is excellent, with higher accuracy and with greater computational efficiency.

I. Introduction

In this paper, we will consider the problem of sound propagation through the APU (Auxiliary Power Unit) exhaust duct, which is typically straight, has multiple annular segments each with a different locally reacting or bulk absorbing liner, and carries a non-uniform mean flow with strong temperature gradients [1]. A suitable approach to compute the propagation for such a geometry is mode-matching, which consists of expressing the acoustic field in each segment as a series of modes, and then determining the modal amplitudes by matching the fields at each interface between two segments by suitable continuity conditions [2].

The system of mode-matching equations results from taking inner-products of the duct eigenfunctions with certain test functions. For uniform flow and temperature, the duct eigenfunctions are Besselfunctions. Since closed form integrals are known for products of Besselfunctions [3], the choice of a suitable set of Besselfunctions as test functions allows us to determine the inner-products analytically exactly. For non-uniform flow and temperature however, the duct eigenfunctions (modal solutions of the Pridmore-Brown equation) are not Besselfunctions anymore, and no exact integrals of products of modes are known. For the classical mode-matching approach a set of Besselfunctions may still be used as test functions, although the inner-products cannot (to our knowledge) be computed in closed form, and numerical quadrature is needed.

In this paper we present a new approach that uses the same Pridmore-Brown modes as test functions, but instead of the standard inner-product we use an associated bilinear form[1] that resembles an "inner-product". We will show that in this way the integrals we need are available in closed form.

*PhD student, National Aerospace Laboratory (NLR), Marknesse, The Netherlands

†Associate Professor, Eindhoven University of Technology (TU/e), Eindhoven, The Netherlands, Senior Member AIAA

‡Senior Scientist, National Aerospace Laboratory (NLR), Marknesse, The Netherlands

[1]Mathematically it is not exactly an inner-product. Although imprecise, we will refer to it here as inner-product because of the role it plays in the mode matching procedure.

The use of this new inner-product for mode-matching may require to compute an extra set of Pridmore-Brown modes to be used as test functions, or the solution of an inhomogeneous Pridmore-Brown equation. Any of these solutions have to be computed only once, regardless of the number of segments, whereas for the classical approach we need to compute all inner-products at each interface. Furthermore, in some occasions the off-diagonal inner-products are zero, which simplify the calculations even more.

Since the computational work is comparable to the numerical quadrature for a single interface while the inherent numerical integration errors are avoided, we conclude that our new approach is both more accurate and cheaper than the classical mode matching methods.

We note that the issue of possible instabilities due to the interaction of shear layer and impedance wall (as for example discussed in [4, 5]) will not be addressed here. Ill-posedness problems associated with a vanishing boundary layer only occur in time domain calculations, while the detection of possible unstable modes requires a causality analysis that we have not undertaken in the present context.

II. Problem Formulation

II.A. General Parallel Flow

We start with linearised Euler equations for time-harmonic modal solutions in general parallel mean flow. Only the mean pressure is assumed constant. If the mean flow is uniform in x-direction and only varies in (y, z), the coefficients of the equations do not depend on x and solutions proportional to $\mathrm{e}^{\mathrm{i}kx}$ (modes) are possible. The resulting equation can be recognised as a preform of the Pridmore-Brown equation.

Although the final application will be for a circular symmetric mean flow in a circular duct, we derive these general equations because later we will derive and use some general results for solutions in the form of analytically exact integrals.

Assume an inviscid, non-heat conducting ideal gas with uniform mean pressure p_0, a parallel mean flow velocity $\boldsymbol{v}_0$ in x-direction with density ρ_0 and sound speed c_0 varying in (y, z) only

$$\boldsymbol{v}_0 = u_0(y,z)\boldsymbol{e}_x, \quad \rho_0 = \rho_0(y,z), \quad c_0 = c_0(y,z), \quad p_0 = \rho_0 \mathcal{R} T_0 = \gamma^{-1}\rho_0 c_0^2 = \text{constant}. \tag{1}$$

It follows from the linearized Euler equations that perturbations (subscript 1) of a parallel mean flow (subscript 0) are governed by

$$\mathrm{D}_0\rho_1 + \boldsymbol{v}_1 \cdot \nabla\rho_0 + \rho_0 \nabla\cdot\boldsymbol{v}_1 = 0, \tag{2a}$$

$$\rho_0\big(\mathrm{D}_0\boldsymbol{v}_1 + \boldsymbol{v}_1\cdot\nabla\boldsymbol{v}_0\big) + \nabla p_1 = \boldsymbol{0}, \tag{2b}$$

$$c_0^2\big(\mathrm{D}_0\rho_1 + \boldsymbol{v}_1\cdot\nabla\rho_0\big) = \mathrm{D}_0 p_1, \tag{2c}$$

where the linearized convective derivative is denoted by $\mathrm{D}_0 = \frac{\partial}{\partial t} + u_0\frac{\partial}{\partial x}$. The convective derivative of the divergence of momentum equation (2b) becomes with mass equation (2a) and again momentum equation (2b)

$$c_0^2\mathrm{D}_0^3\rho_1 + 2c_0^2\tfrac{\partial}{\partial x}\big(\nabla u_0\cdot\nabla p_1\big) - \mathrm{D}_0(c_0^2\nabla^2 p_1) = 0. \tag{3}$$

Since $c_0^2(\mathrm{D}_0\boldsymbol{v}_1\cdot\nabla\rho_0) = \nabla c_0^2\cdot\nabla p_1$, we have with (2c) finally (*c.f.* [6])

$$\mathrm{D}_0^3 p_1 + 2c_0^2\tfrac{\partial}{\partial x}\big(\nabla u_0\cdot\nabla p_1\big) - \mathrm{D}_0\nabla\cdot\big(c_0^2\nabla p_1\big) = 0 \tag{4}$$

If we look for solutions of the form $p_1(x, y, z, t) = P(y, z)\,\mathrm{e}^{\mathrm{i}kx-\mathrm{i}\omega t}$ we obtain a preform of the Pridmore-Brown equation [7, 8]

$$\mathrm{i}\Omega^3 P + 2\mathrm{i}kc_0^2\,(\nabla u_0\cdot\nabla P) + \mathrm{i}\Omega\left(-k^2c_0^2P + \nabla\cdot\left(c_0^2\nabla P\right)\right) = 0, \tag{5}$$

where

$$\Omega = \omega - ku_0.$$

By noting that $-k\nabla u_0 = \nabla\Omega$ this equation can be further simplified to

$$\nabla\cdot\left(\frac{c_0^2}{\Omega^2}\nabla P\right) + \left(1 - \frac{k^2c_0^2}{\Omega^2}\right)P = 0. \tag{6}$$

If $u_0 \equiv 0$, this reduces to

$$\nabla\cdot\left(c_0^2\nabla P\right) + \left(\omega^2 - k^2c_0^2\right)P = 0, \tag{7}$$

which is just equivalent to the Helmholtz equation if c_0 is constant.

II.B. Circular Symmetric Mean Flow in Circular Duct

The final application will be for a circular symmetric mean flow in a circular duct with radius d, which models an APU exhaust duct (Fig. 1). Therefore, we will develop the equations in cylindrical coordinates and consider Fourier modes in the circumferential coordinate.

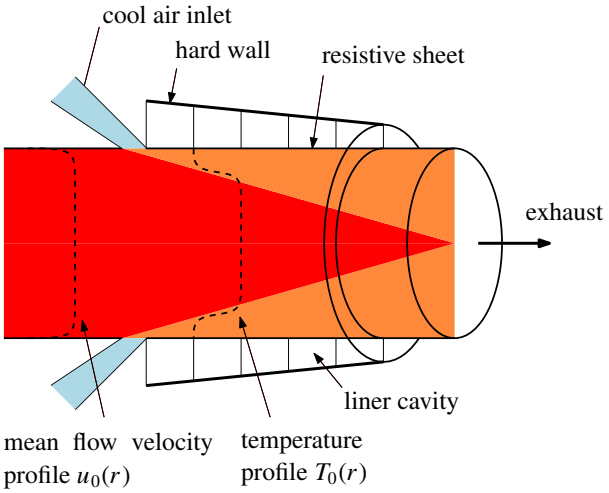

Figure 1. APU geometry.

In a radially symmetric mean flow $u_0(r), \rho_0(r), c_0(r)$ with perturbations $\boldsymbol{v}_1 = u_1\boldsymbol{e}_x + v_1\boldsymbol{e}_r + w_1\boldsymbol{e}_\theta$, ρ_1, p_1 of the form

$$(u_1, v_1, w_1, \rho_1, p_1) = (U, V, W, R, P)\,\mathrm{e}^{-\mathrm{i}\omega t + \mathrm{i}kx + \mathrm{i}m\theta}, \tag{8}$$

we have the equations

$$-\mathrm{i}\Omega R + \rho_0\left(\mathrm{i}kU + V' + \frac{1}{r}V + \frac{\mathrm{i}m}{r}W\right) + \rho_0' V = 0, \tag{9a}$$

$$\rho_0\left(-\mathrm{i}\Omega U + u_0' V\right) + \mathrm{i}kP = 0, \tag{9b}$$

$$-\mathrm{i}\Omega\rho_0 V + P' = 0, \tag{9c}$$

$$-\mathrm{i}\Omega\rho_0 W + \frac{\mathrm{i}m}{r}P = 0, \tag{9d}$$

$$c_0^2\left(-\mathrm{i}\Omega R + \rho_0' V\right) + \mathrm{i}\Omega P = 0, \tag{9e}$$

where a prime denotes a derivative to r. R can be eliminated by replacing equations (9a) and (9e) by

$$\rho_0 c_0^2\left(\mathrm{i}kU + V' + \frac{1}{r}V + \frac{\mathrm{i}m}{r}W\right) - \mathrm{i}\Omega P = 0, \tag{9f}$$

This system can be reduced to one equation for P, known as the Pridmore-Brown equation

$$\frac{\Omega^2}{rc_0^2}\left(\frac{rc_0^2P'}{\Omega^2}\right)' + \left(\frac{\Omega^2}{c_0^2} - k^2 - \frac{m^2}{r^2}\right)P = 0. \tag{10}$$

which is to be compared with (6). Another form is

$$P'' + \left(\frac{1}{r} + \frac{T_0'}{T_0} + 2\frac{ku_0'}{\Omega}\right)P' + \left(\frac{\Omega^2}{c_0^2} - k^2 - \frac{m^2}{r^2}\right)P = 0. \tag{11}$$

II.C. Boundary Conditions

Owing to the origin of the present problem (sound propagation in an APU), the boundary conditions may involve locally reacting liners and bulk absorbers. In its generality, however, all this is not relevant for the present paper. So we only briefly sketch how the locally and bulk absorbing liners are modeled by means of the boundary equations for the Pridmore-Brown equation [9]. In the end we will only use an impedance condition.

Since we want to include cases with slipping flow (like for example uniform flow), we use the Ingard-Myers boundary condition for a boundary layer with vanishing thickness (modeled as a vortex sheet) along a straight wall [10]. This is for time harmonic perturbations

$$-\mathrm{i}\omega(\boldsymbol{v}_1\cdot\boldsymbol{n}) = (-\mathrm{i}\omega + \boldsymbol{v}_0\cdot\nabla)\frac{p_1}{Z}. \tag{12}$$

In principle, this boundary condition can be used for both locally and non-locally reacting (bulk absorbing) liners, with the proviso that for a non-locally reacting liner Z depends on the axial wavenumber k, or in other words, on the angle of incidence of the field. In this paper we only consider locally reacting liners with just a constant Z. For a circularly cylindrical duct, after elimination of the radial velocity, (12) becomes

$$P' - \frac{\mathrm{i}\rho_0\Omega^2}{\omega Z}P = 0 \qquad \text{at } r = d. \tag{13}$$

III. Exact Integrals of Pridmore-Brown Eigenfunctions

III.A. Exact Integrals of Solutions of the Helmholtz Equation

Mode-matching is a particularly successful method for acoustic wave propagation in segmented ducts of circular or rectangular cross section with a uniform medium. The necessary integrals of the modal eigenfunctions (Bessel functions or (co)sine functions) appear to be available in closed form, which greatly simplifies the numerical evaluation. These closed form integrals are a manifestation of a more general property of solutions of the Helmholtz equation. Suppose we have, for parameters α and β the solutions ϕ and ψ in a region $\mathcal{A} \in \mathbb{R}^2$ with boundary Γ (as yet, boundary conditions do not play a role) of

$$\nabla^2\phi + \alpha^2\phi = 0, \tag{14a}$$

$$\nabla^2\psi + \beta^2\psi = 0. \tag{14b}$$

When we subtract ϕ times the second equation from ψ times the first and integrate over $\mathcal{A}$ we obtain

$$(\alpha^2 - \beta^2)\iint_{\mathcal{A}} \phi\psi\,\mathrm{d}S = \iint_{\mathcal{A}} \left(\phi\nabla^2\psi - \psi\nabla^2\phi\right)\mathrm{d}S = \iint_{\mathcal{A}} \nabla\cdot\left(\phi\nabla\psi - \psi\nabla\phi\right)\mathrm{d}S. \tag{15}$$

After using the divergence theorem, this inner-product of ϕ and ψ are given by an integral along the boundary

$$\iint_{\mathcal{A}} \phi\psi\,\mathrm{d}S = \frac{1}{\alpha^2 - \beta^2}\int_{\Gamma} \left(\phi\nabla\psi\cdot\boldsymbol{n} - \psi\nabla\phi\cdot\boldsymbol{n}\right)\mathrm{d}\ell. \tag{16}$$

If $\alpha = \beta$, this result can not be used. Suppose that we replace equation (14b) by the far more general

$$\nabla^2\chi + \alpha^2\chi = f, \tag{17}$$

where f is an arbitrary (integrable) function. When we again cross-wise multiply and subtract as before, we find

$$\iint_{\mathcal{A}} \phi f\,\mathrm{d}S = \iint_{\mathcal{A}} \left(\phi\nabla^2\chi - \chi\nabla^2\phi\right)\mathrm{d}S = \int_{\Gamma} \left(\phi\nabla\chi\cdot\boldsymbol{n} - \chi\nabla\phi\cdot\boldsymbol{n}\right)\mathrm{d}\ell. \tag{18}$$

This result was derived without specifying any boundary conditions on χ, so they can be chosen arbitrarily as long as there *exists* a solution χ. This is guaranteed[2] if (the boundary conditions on χ are such, that) α is not an eigenvalue of the homogeneous version of equation (17).

The advantage of this result is its generality. We can substitute for f any function we need, for example $f = \phi$, solution of (14a). The disadvantage is of course, that it requires the solution of the additional inhomogeneous equation (17). So in practice we will use this result only if (16) breaks down.

In the specific case of a circular disk of radius 1 and circularly symmetric solutions $\phi = J_m(\alpha r)\,\mathrm{e}^{\mathrm{i}m\theta}$ and $\psi = J_m(\beta r)\,\mathrm{e}^{-\mathrm{i}m\theta}$ (we choose opposite signs of $\mathrm{i}m\theta$ for non-trivial results later), substituted in (16), we obtain the well-known [3] relation for Besselfunctions

$$\int_0^1 J_m(\alpha r)\,J_m(\beta r)\,r\mathrm{d}r = \frac{1}{\alpha^2-\beta^2}\left[\beta\,J_m(\alpha)\,J_m'(\beta) - \alpha\,J_m'(\alpha)\,J_m(\beta)\right]. \tag{19}$$

For the case when $\alpha = \beta$ one approach is to take the limit and use l'Hôpital's rule, with result

$$\int_0^1 J_m(\alpha r)^2 r\,\mathrm{d}r = \frac{1}{2}\left(1-\frac{m^2}{\alpha^2}\right)J_m(\alpha)^2 + \frac{1}{2}J_m'(\alpha)^2. \tag{20}$$

A more generic approach is the one discussed above. Suppose that we have $\chi(r,\theta) = \hat{\chi}(r)\,\mathrm{e}^{-\mathrm{i}m\theta}$, regular in $r = 0$, where $\hat{\chi}$ is a solution of the inhomogeneous Bessel equation

$$\frac{1}{r}(r\hat{\chi}')' + \left(\alpha^2 - \frac{m^2}{r^2}\right)\hat{\chi} = J_m(\alpha r), \tag{21}$$

(for example $\hat{\chi}(r) = -rJ_m'(\alpha r)/2\alpha$), then we have the equivalent result

$$\int_0^1 J_m(\alpha r)^2 r\mathrm{d}r = J_m(\alpha)\hat{\chi}'(1) - \alpha J_m'(\alpha)\hat{\chi}(1). \tag{22}$$

Again, the boundary conditions on χ can be selected arbitrarily, except for the restriction that $A\hat{\chi}(1) + B\hat{\chi}'(1) \neq 0$ if $AJ_m(\alpha) + \alpha B J_m'(\alpha) = 0$.

The above manipulations (14)-(18) can be repeated for (7) (with $u_0 \equiv 0$) to obtain weighted inner-product integrals of the type

$$\iint_{\mathcal{A}} c_0^2 P\tilde{P}\,\mathrm{d}S$$

but for the general case (6) this is not possible because $\Omega = \Omega(k)$. Indeed, no closed form expressions can be found for the standard inner-products with eigenfunctions of the Pridmore-Brown equation, which are required to set up the mode-matching equations, so it seems that we have to resort to numerical quadrature to compute the integrals. With increasing radial order the eigenfunctions become more and more oscillatory, resulting in increasingly more difficult numerical computations.

All this is not the case, if we change the standard inner-product integrals into a dedicated integral, associated to the prevailing equations, which we call (as it is not a real inner-product) a bilinear form.

In the following we will construct two bilinear forms consisting of products of eigenfunctions. One for the general case of parallel mean flow (applicable for example in distortion mode problems [12]), much in the same fashion as discussed above, and one for the particular case of circular ducts with radially symmetric mean flow, the so-called Pridmore-Brown modes. These results may be used to compute the coefficients of mode-matching equations in closed form. A numerical implementation will be given, and some numerical examples comparing the classic approach and the present new one.

This result was inspired by [13], where a related integral was used to obtain a solvability condition for a multiple scales solution of the disturbance field for a slowly varying duct with mean swirling flow.

[2]This result is related to the Fredholm alternative for linear operators [11]. Assume that $A\chi = B\nabla\chi\cdot\boldsymbol{n}$ on Γ and suppose that there exists a nonzero solution w of $\nabla^2 w + \alpha^2 w = 0$ with the same boundary conditions. Then we obtain the, for arbitrary f, contradiction $\iint_{\mathcal{A}} wf\,\mathrm{d}S = \int_\Gamma (w\nabla\chi\cdot\boldsymbol{n} - \chi\nabla w\cdot\boldsymbol{n})\,\mathrm{d}\ell = 0$.

III.B. Exact Integrals of Parallel-Flow Modal Eigenfunctions

Analogous to (16) we want to construct an integral involving products of Pridmore-Brown eigenfunctions and use the divergence theorem to evaluate its value through the eigenfunction values on the boundary. Suppose that we have parallel mean flow in x-direction and modes of the form

$$[\rho_1,\, p_1,\, \boldsymbol{v}_1] = [R(y,z),\, P(y,z),\, U(y,z)\boldsymbol{e}_x + V(y,z)\boldsymbol{e}_y + W(y,z)\boldsymbol{e}_z]\,\mathrm{e}^{\mathrm{i}kx-\mathrm{i}\omega t}\,. \tag{23}$$

U, V and W are the velocity components in the x, y and z direction of a Cartesian coordinate system. For modal solutions of this form which are governed by (2) we have

$$-\mathrm{i}\Omega P + i\rho_0 c_0^2 kU + \rho_0 c_0^2 (V_y + W_z) = 0, \tag{24a}$$
$$-\mathrm{i}\rho_0\Omega U + \rho_0\left(u_{0y}V + u_{0z}W\right) + \mathrm{i}kP = 0, \tag{24b}$$
$$-\mathrm{i}\rho_0\Omega V + P_y = 0, \tag{24c}$$
$$-\mathrm{i}\rho_0\Omega W + P_z = 0, \tag{24d}$$

where $\Omega = \omega - ku_0$, and R follows directly from the other amplitudes, for example with 2c. (Note that the system reduces to (6) if U, V and W are eliminated.) Together with suitable boundary conditions this is an eigenvalue problem with eigenvalue k, but this will not be used here; k will be considered as a given constant.

When the individual equations in (24) are multiplied by suitable combinations[3] of other solutions of the same equations (say $\tilde{P}$, $\tilde{U}$, $\tilde{V}$ and $\tilde{W}$) with constant $\tilde{k}$ and corresponding auxiliary function $\tilde{\Omega} = \omega - \tilde{k}u_0$, and subsequently added together, we obtain:

$$\begin{aligned}\left(-\mathrm{i}\Omega P + \mathrm{i}\rho_0 c_0^2 kU + \rho_0 c_0^2 V_y + \rho_0 c_0^2 W_z\right)\frac{\tilde{P}}{\rho_0 c_0^2} + \left(-\mathrm{i}\Omega\rho_0 U + \rho_0 u_{0y}V + \rho_0 u_{0z}W + \mathrm{i}kP\right)\frac{\tilde{k}\tilde{P}}{\rho_0\tilde{\Omega}}\\ - \left(-\mathrm{i}\Omega\rho_0 V + P_y\right)\tilde{V} - \left(-\mathrm{i}\Omega\rho_0 W + P_z\right)\tilde{W} = 0\end{aligned} \tag{25}$$

After reordering and splitting off a cross-wise divergence, this is equivalent to

$$\begin{aligned}-\mathrm{i}\left(\frac{\Omega}{\rho_0 c_0^2} - \frac{k\tilde{k}}{\rho_0\tilde{\Omega}}\right)\tilde{P}P - \mathrm{i}\frac{\Omega\tilde{k} - \tilde{\Omega}k}{\tilde{\Omega}}\tilde{P}U + \mathrm{i}\rho_0\Omega(\tilde{V}V + \tilde{W}W) - V\tilde{P}_y - W\tilde{P}_z + \left(\tilde{V}_y + \tilde{W}_z\right)P\\ + \frac{\tilde{k}}{\tilde{\Omega}}\left(u_{0y}\tilde{V} + u_{0z}\tilde{W}\right)P + \tilde{\Omega}\left(\frac{\tilde{P}V - \tilde{V}P}{\tilde{\Omega}}\right)_y + \tilde{\Omega}\left(\frac{\tilde{P}W - \tilde{W}P}{\tilde{\Omega}}\right)_z = 0.\end{aligned} \tag{26}$$

After using the defining equations (24) this becomes

$$\begin{aligned}-\mathrm{i}\left(\frac{\Omega}{\rho_0 c_0^2} - \frac{k\tilde{k}}{\rho_0\tilde{\Omega}}\right)\tilde{P}P - \mathrm{i}\frac{\Omega\tilde{k} - \tilde{\Omega}k}{\tilde{\Omega}}\tilde{P}U + \mathrm{i}\rho_0\Omega(\tilde{V}V + \tilde{W}W) - \mathrm{i}\tilde{\Omega}\rho_0(\tilde{V}V + \tilde{W}W)\\ + \mathrm{i}\left(\frac{\tilde{\Omega}}{\rho_0 c_0^2} - \frac{\tilde{k}^2}{\rho_0\tilde{\Omega}}\right)\tilde{P}P + \tilde{\Omega}\left(\frac{\tilde{P}V - \tilde{V}P}{\tilde{\Omega}}\right)_y + \tilde{\Omega}\left(\frac{\tilde{P}W - \tilde{W}P}{\tilde{\Omega}}\right)_z = 0.\end{aligned} \tag{27}$$

Recombining and dividing by $\tilde{\Omega}$ yields

$$\begin{aligned}-\mathrm{i}(k-\tilde{k})\frac{1}{\tilde{\Omega}}\left[\left(\frac{u_0}{\rho_0 c_0^2} + \frac{\tilde{k}}{\rho_0\tilde{\Omega}}\right)\tilde{P}P + \frac{\omega}{\tilde{\Omega}}\tilde{P}U - \rho_0 u_0(\tilde{V}V + \tilde{W}W)\right] =\\ \frac{\partial}{\partial y}\left(\frac{\tilde{P}V - \tilde{V}P}{\tilde{\Omega}}\right) + \frac{\partial}{\partial z}\left(\frac{\tilde{P}W - \tilde{W}P}{\tilde{\Omega}}\right).\end{aligned} \tag{28}$$

[3]This choice is clearly not self-evident, and not the result of random trying. It was found by first taking the products of the governing equations with arbitrary functions, and then imposing the required conditions on these functions. The resulting equations appeared to be equivalent to our original equations for P, U, V and W.

In case we want to write the left hand side in terms of P only, we can use the defining equations for U, V and W. When we integrate (28) over a cross section $\mathcal{A}$ with boundary Γ and use the divergence theorem, we obtain an integral over $\mathcal{A}$ of parallel-flow shape functions, in particular (with suitable boundary conditions and eigenvalues k) parallel-flow eigenfunctions, expressed as an integral along boundary Γ. We introduce the vector of shape functions $\boldsymbol{F} = \left[P, U, V, W\right]$ and denote this integral by[4]

$$\langle\!\langle \boldsymbol{F}, \tilde{\boldsymbol{F}} \rangle\!\rangle = \iint_{\mathcal{A}} \frac{1}{\tilde{\Omega}} \left[\left(\frac{u_0}{\rho_0 c_0^2} + \frac{\tilde{k}}{\rho_0 \tilde{\Omega}} \right) \tilde{P} P + \frac{\omega}{\tilde{\Omega}} \tilde{P} U - \rho_0 u_0 (\tilde{V} V + \tilde{W} W) \right] \mathrm{d}S$$
$$= \frac{\mathrm{i}}{k - \tilde{k}} \int_{\Gamma} \frac{\tilde{P}(V n_y + W n_z) - (\tilde{V} n_y + \tilde{W} n_z) P}{\tilde{\Omega}} \, \mathrm{d}\ell, \quad (29)$$

where n_y and n_z denote the y and z components of the outward normal vector on Γ and $k \neq \tilde{k}$.

If $u_0 \equiv 0$ this reduces to a regular integral innerproduct (with a weight function $\propto \rho_0^{-1} \propto c_0^2$)

$$\langle\!\langle \boldsymbol{F}, \tilde{\boldsymbol{F}} \rangle\!\rangle = \frac{k + \tilde{k}}{\omega^2} \iint_{\mathcal{A}} \frac{\tilde{P} P}{\rho_0} \, \mathrm{d}S = \frac{1}{(k - \tilde{k})\omega^2} \int_{\Gamma} \frac{\tilde{P}(P_y n_y + P_z n_z) - (\tilde{P}_y n_y + \tilde{P}_z n_z) P}{\rho_0} \, \mathrm{d}\ell, \quad (30)$$

a result, very similar to (16), and which could have been obtained directly from (7).

For a slipping mean flow along an impedance wall at Γ we apply Ingard-Myers conditions $V n_y + W n_z = \Omega P / \omega Z$ and $\tilde{V} n_y + \tilde{W} n_z = \tilde{\Omega} \tilde{P} / \omega \tilde{Z}$ and obtain

$$\langle\!\langle \boldsymbol{F}, \tilde{\boldsymbol{F}} \rangle\!\rangle = \frac{\mathrm{i}}{k - \tilde{k}} \int_{\Gamma} \frac{\tilde{P} P}{\tilde{\Omega} \omega} \left(\frac{\Omega}{Z} - \frac{\tilde{\Omega}}{\tilde{Z}} \right) \mathrm{d}\ell. \quad (31)$$

The integrals vanish for hard walls, when $Z = \tilde{Z} = \infty$. For a no-slip mean flow with $u_0 = 0$ along Γ and impedance boundary conditions $P = Z(V n_y + W n_z)$ and $\tilde{P} = \tilde{Z}(\tilde{V} n_y + \tilde{W} n_z)$, we obtain

$$\langle\!\langle \boldsymbol{F}, \tilde{\boldsymbol{F}} \rangle\!\rangle = \frac{\mathrm{i}}{k - \tilde{k}} \int_{\Gamma} \frac{\tilde{P} P}{\omega} \left(\frac{1}{Z} - \frac{1}{\tilde{Z}} \right) \mathrm{d}\ell. \quad (32)$$

Interestingly, the integral vanishes for different modes that correspond with the same Z.

Although this surface integral resembles a non-standard inner-product between vectors $\boldsymbol{F}$ and $\tilde{\boldsymbol{F}}$, it is not an inner product because it lacks positive-definiteness for $\langle\!\langle \boldsymbol{F}, \boldsymbol{F} \rangle\!\rangle$, mainly because of the PU term. Therefore, we refer to it as a bilinear map, although occasionally, because it plays the same role of an inner product as in the classical mode matching procedure, it may be referred to as an inner-product.

The above result is evidently not valid for $k = \tilde{k}$. In practice, when we deal with modal eigenfunctions, all satisfying the same boundary condition, the limit of $k = \tilde{k}$ goes together with $\boldsymbol{F} = \tilde{\boldsymbol{F}}$ and we will consider that situation here.

We start with the following associated inhomogeneous system of (24) with solution $[\hat{P}, \hat{U}, \hat{V}, \hat{W}]$, with the same k as in the original system, and a solution vector $[P, U, V, W]$ satisfying (24).

$$-\mathrm{i}\Omega \hat{P} + \mathrm{i}\rho_0 c_0^2 k \hat{U} + \rho_0 c_0^2 (\hat{V}_y + \hat{W}_z) = \mathrm{i}(u_0 P + \rho_0 c_0^2 U), \quad (33a)$$
$$-\mathrm{i}\Omega \rho_0 \hat{U} + \rho_0 u_{0y} \hat{V} + \rho_0 u_{0z} \hat{W} + \mathrm{i}k \hat{P} = \mathrm{i}(\rho_0 u_0 U + P), \quad (33b)$$
$$-\mathrm{i}\Omega \rho_0 \hat{V} + \hat{P}_y = \mathrm{i}\rho_0 u_0 V, \quad (33c)$$
$$-\mathrm{i}\Omega \rho_0 \hat{W} + \hat{P}_z = \mathrm{i}\rho_0 u_0 W, \quad (33d)$$

with boundary conditions such, that k is not an eigenvalue of the left hand side, in order to guarantee the existence of a solution $[\hat{P}, \hat{U}, \hat{V}, \hat{W}]$.

[4] If a symmetric form is preferred, we can replace $\langle\!\langle \boldsymbol{F}, \tilde{\boldsymbol{F}} \rangle\!\rangle$ by $\frac{1}{2}\langle\!\langle \boldsymbol{F}, \tilde{\boldsymbol{F}} \rangle\!\rangle + \frac{1}{2}\langle\!\langle \tilde{\boldsymbol{F}}, \boldsymbol{F} \rangle\!\rangle$ and the RHS correspondingly.

We multiply left and right hand sides with $P/\rho_0 c_0^2$, $kP/\rho_0\Omega$, $-V$ and $-W$ respectively, add, and do exactly the same manipulations as before. We find that the factor $k-\tilde{k}$ vanishes, and obtain the final result

$$\langle\!\langle \boldsymbol{F},\boldsymbol{F} \rangle\!\rangle = \iint\limits_{\mathcal{A}} \frac{1}{\Omega}\left[\left(\frac{u_0}{\rho_0 c_0^2}+\frac{k}{\rho_0\Omega}\right)P^2+\frac{\omega}{\Omega}UP-\rho_0 u_0(V^2+W^2)\right]\mathrm{d}S$$
$$= \mathrm{i}\int\limits_{\Gamma}\frac{\hat{P}(Vn_y+Wn_z)-(\hat{V}n_y+\hat{W}n_z)P}{\Omega}\,\mathrm{d}\ell. \quad (34)$$

If $u_0 \equiv 0$ we obtain

$$\langle\!\langle \boldsymbol{F},\boldsymbol{F} \rangle\!\rangle = \frac{2k}{\omega^2}\iint\limits_{\mathcal{A}}\frac{P^2}{\rho_0}\,\mathrm{d}S = \frac{1}{\omega^2}\int\limits_{\Gamma}\frac{\hat{P}(P_y n_y+P_z n_z)-(\hat{P}_y n_y+\hat{P}_z n_z)P}{\rho_0}\,\mathrm{d}\ell. \quad (35)$$

III.C. Exact Integrals of Radial Pridmore-Brown Modes

A special application of the above results will be for a circularly symmetric mean flow $u_0(r)$, $c_0(r)$, $\rho_0(r)$ in a circular duct of radius d and cross section $\mathcal{A}$ (an annular duct would require only little changes) with polar coordinate system (x,r,θ) and $\boldsymbol{v}_1 = u\boldsymbol{e}_x + v\boldsymbol{e}_r + w\boldsymbol{e}_\theta$. In this case the solution can be written as a sum over circumferential Fourier modes, and we can assume modal shape solutions of the form $\boldsymbol{F}(r)\,\mathrm{e}^{\mathrm{i}m\theta} = [P(r), U(r), V(r), W(r)]\,\mathrm{e}^{\mathrm{i}m\theta}$, satisfying

$$-\mathrm{i}\Omega P + \mathrm{i}\rho_0 c_0^2 kU + \rho_0 c_0^2\Big(V' + \frac{1}{r}V + \frac{\mathrm{i}m}{r}W\Big) = 0, \quad (36a)$$
$$-\mathrm{i}\rho_0\Omega U + \rho_0 u_0' V + \mathrm{i}kP = 0, \quad (36b)$$
$$-\mathrm{i}\rho_0\Omega V + P' = 0, \quad (36c)$$
$$-\mathrm{i}\rho_0\Omega W + \frac{\mathrm{i}m}{r}P = 0, \quad (36d)$$

where $\Omega = \omega - ku_0$ and the $'$ denotes an r-derivative. As before, we will assume k to be just a constant, but with suitable boundary conditions this system is an eigenvalue problem with eigenvalue k.

Due to the symmetry, it is no restriction to assume another solution of (36) with $\tilde{k} \neq k$, of the form $\tilde{\boldsymbol{F}}(r)\,\mathrm{e}^{-\mathrm{i}m\theta} = [\tilde{P}(r), \tilde{U}(r), \tilde{V}(r), -\tilde{W}(r)]\,\mathrm{e}^{-\mathrm{i}m\theta}$, such that the surface integral in (29) (divided by 2π) simplifies to

$$\langle \boldsymbol{F}, \tilde{\boldsymbol{F}}\rangle = \int\limits_0^d \frac{r}{\tilde{\Omega}}\left[\left(\frac{u_0}{\rho_0 c_0^2}+\frac{\tilde{k}}{\rho_0\tilde{\Omega}}\right)P\tilde{P}+\frac{\omega}{\tilde{\Omega}}U\tilde{P}-\rho_0 u_0(V\tilde{V}+W\tilde{W})\right]\mathrm{d}r = \frac{\mathrm{i}d}{k-\tilde{k}}\left[\frac{\tilde{P}V-\tilde{V}P}{\tilde{\Omega}}\right]_{r=d}, \quad (37)$$

where we assumed that the solutions are regular in $r=0$.

If $u_0 \equiv 0$ we obtain

$$\langle \boldsymbol{F}, \tilde{\boldsymbol{F}}\rangle = \frac{k+\tilde{k}}{\omega^2}\int\limits_0^d \frac{r}{\rho_0}P\tilde{P}\,\mathrm{d}r = \frac{d}{(k-\tilde{k})\omega}\left[\frac{\tilde{P}P'-\tilde{P}'P}{\rho_0}\right]_{r=d}, \quad (38)$$

With slipping flow and impedance walls along $r=d$ we apply Ingard-Myers boundary conditions $V = \Omega P/\omega Z$ and $\Omega = \omega - ku_0(d)$ for both solutions, and obtain

$$\langle \boldsymbol{F}, \tilde{\boldsymbol{F}}\rangle = \frac{\mathrm{i}d\tilde{P}P}{(k-\tilde{k})\tilde{\Omega}\omega}\left(\frac{\Omega}{Z}-\frac{\tilde{\Omega}}{\tilde{Z}}\right), \quad (39)$$

which vanishes if $Z = \tilde{Z} = \infty$. With no-slip flow and $u_0(d) = 0$ this simplifies to

$$\langle \boldsymbol{F}, \tilde{\boldsymbol{F}}\rangle = \frac{\mathrm{i}d\tilde{P}P}{(k-\tilde{k})\omega}\left(\frac{1}{Z}-\frac{1}{\tilde{Z}}\right).$$

If k and $\tilde{k}$ are different eigenvalues from the same impedance condition, so $\tilde{Z} = Z$, then all integrals vanish in this case.

To find the degenerate case of $\tilde{k} = k$ and $\tilde{\boldsymbol{F}} = \boldsymbol{F}$, we consider with constant k the solution $\boldsymbol{F}\,\mathrm{e}^{-\mathrm{i}m\theta} = [P, U, V, -W]\,\mathrm{e}^{-\mathrm{i}m\theta}$ (equally given by (36)) and the associated solution $\hat{\boldsymbol{F}}\,\mathrm{e}^{-\mathrm{i}m\theta} = [\hat{P}, \hat{U}, \hat{V}, -\hat{W}]\,\mathrm{e}^{-\mathrm{i}m\theta}$ of the inhomogeneous system (with the same k)

$$-\mathrm{i}\Omega\hat{P} + \mathrm{i}\rho_0 c_0^2 k\hat{U} + \rho_0 c_0^2\left(\hat{V}' + \frac{1}{r}\hat{V} + \frac{\mathrm{i}m}{r}\hat{W}\right) = \mathrm{i}(u_0 P + \rho_0 c_0^2 U) \tag{40a}$$

$$-\mathrm{i}\Omega\rho_0\hat{U} + \rho_0 u_0'\hat{V} + \mathrm{i}k\hat{P} = \mathrm{i}(\rho_0 u_0 U + P) \tag{40b}$$

$$-\mathrm{i}\Omega\rho_0\hat{V} + \hat{P}' = \mathrm{i}\rho_0 u_0 V \tag{40c}$$

$$-\mathrm{i}\Omega\rho_0\hat{W} + \frac{\mathrm{i}m}{r}\hat{P} = \mathrm{i}\rho_0 u_0 W \tag{40d}$$

In actual practice, the system (40) will be reduced to the following inhomogeneous Pridmore-Brown equation in $\hat{P}$, which may be solved by almost the same routine as is used for the Pridmore-Brown equation itself.

$$\frac{\Omega^2}{rc_0^2}\left(\frac{rc_0^2}{\Omega^2}\hat{P}'\right)' + \left(\frac{\Omega^2}{c_0^2} - k^2 - \frac{m^2}{r^2}\right)\hat{P} = 2\frac{\omega u_0'}{\Omega^2}P' - 2\left(\frac{u_0\Omega}{c_0^2} + k\right)P \tag{41}$$

The surface integral (divided by 2π) of (34) now simplifies to

$$\langle \boldsymbol{F}, \boldsymbol{F}\rangle = \int_0^d \frac{r}{\Omega}\left[\left(\frac{u_0}{\rho_0 c_0^2} + \frac{k}{\rho_0\Omega}\right)P^2 + \frac{\omega}{\Omega}UP - \rho_0 u_0(V^2 + W^2)\right]\mathrm{d}r = \mathrm{i}d\left[\frac{\hat{P}V - \hat{V}P}{\Omega}\right]_{r=d} \tag{42}$$

where we assumed that the solutions are regular in $r = 0$. As before, it should be noted that the inhomogeneous equation (41) has no solutions if the problem for P is an eigenvalue problem with homogeneous boundary conditions, and the same conditions are applied to $\hat{P}$.

If $u_0 \equiv 0$ we obtain

$$\langle \boldsymbol{F}, \boldsymbol{F}\rangle = \frac{2k}{\omega^2}\int_0^d \frac{r}{\rho_0}P^2\,\mathrm{d}r = \frac{d}{\omega^2}\left[\frac{\hat{P}P' - \hat{P}'P}{\rho_0}\right]_{r=d}. \tag{43}$$

IV. Mode-Matching

IV.A. Construction of Matrix Equations (Classical Mode-Matching)

We consider a duct that is divided in N axial segments, and assume that the wall properties are constant within each segment.

We assume that the perturbation field for each segment can be expressed as a summation of eigenmodes of the Pridmore-Brown equation, as discussed previously. This is not obvious and in fact generally not true. Our representation with modes proportional to $\mathrm{e}^{\mathrm{i}kx}$ can be justified [5] by considering it as a Fourier transform in x. The obtained solution in k can be transformed back to x-domain by inverse Fourier transformation. The residues of the poles in the complex k plane then become the modes that were anticipated. In shear flow, however, there are more singularities in k than just the modal poles. There is also a branch cut, also known as "the continuous spectrum" of values of k with $\Omega = \omega - ku_0 = 0$ at (so-called) critical layers, which cannot be evaluated as modes. This contribution is in the present model ignored as it can be shown, as has been reported in [5], that in general it is small.

To compute the field inside the entire duct we set up a system of equations which relates the modal amplitudes in adjacent segments by applying suitable continuity conditions at the interface between them. This is the mode-matching method. Subsequently, we compute the amplitudes in all segments with the aid of the numerically stable S-matrix formalism, as described in the next section.

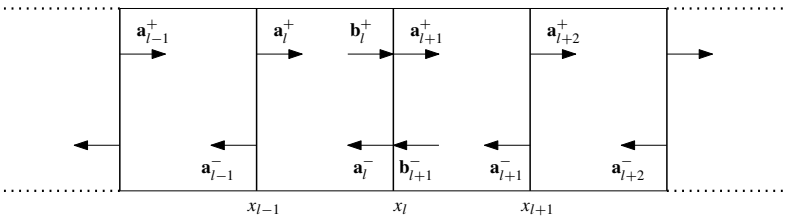

Figure 2. Mode-matching at several interfaces.

In this section we describe the classical mode-matching (CMM) approach based on continuity of pressure and axial velocity. The total field for a given circumferential wavenumber m in each segment is a superposition of all right and left-running modes:

$$p_l(x,r) = \sum_{\mu=1}^{\infty}\Big(a^+_{l,\mu}P^+_{l,\mu}(r)\,\mathrm{e}^{\mathrm{i}k^+_{l,\mu}(x-x_{l-1})} + a^-_{l,\mu}P^-_{l,\mu}(r)\,\mathrm{e}^{\mathrm{i}k^-_{l,\mu}(x-x_l)}\Big), \quad x_{l-1}\leqslant x\leqslant x_l. \tag{44}$$

In a numerical implementation this infinite series has to be truncated; the finite number of modes μ_l to represent the field of the l-th segment depends in general on the type of liner (bulk or locally reacting). At the interface at $x = x_l$ (see Figure 2) we have for the pressure in segment l:

$$p_l(r) = \sum_{\mu=1}^{\mu_l}\Big(b^+_{l,\mu}P^+_{l,\mu}(r) + a^-_{l,\mu}P^-_{l,\mu}(r)\Big). \tag{45}$$

Consider the hard-wall uniform flow eigenfunctions by $\Psi_\nu(r) = J_m(\alpha_\nu r)$ where α_ν are the hard-wall radial wavenumbers, which satisfy $\Psi'_\nu(d) = 0$. These functions form a complete L_2-basis, are at least locally, for high orders, similar in behavior as the Pridmore-Brown modes, and are therefore suitable to serve as test functions when we set up the matrix system for the modal vectors.

Imposing continuity of pressure (approximated due to the truncation) at an interface at x_l and subsequent projection onto the set of test functions Ψ_ν, $\nu = 1,\ldots,\nu^{\max}$, yields

$$\sum_{\mu=1}^{\mu_l} b^+_{l,\mu}(P^+_{l,\mu},\Psi_\nu) + a^-_{l,\mu}(P^-_{l,\mu},\Psi_\nu) = \sum_{\mu=1}^{\mu_{l+1}} a^+_{l+1,\mu}(P^+_{l+1,\mu},\Psi_\nu) + b^-_{l+1,\mu}(P^-_{l+1,\mu},\Psi_\nu), \tag{46}$$

where we use the standard inner-product

$$(f,g) = \int_0^d f(r)g(r)r\,\mathrm{d}r.$$

The set of equations for the continuity of axial velocity is found analogously by using the relation

$$U = \frac{k}{\rho_0\Omega}P - \frac{u'_0}{\rho_0\Omega^2}P', \tag{47}$$

which follows from (9c) and (9b). All matching conditions together yield the following system of equations:

$$\begin{bmatrix}\mathbf{A}^+ & \mathbf{A}^-\\ \mathbf{C}^+ & \mathbf{C}^-\end{bmatrix}\begin{bmatrix}\mathbf{b}^+_l\\ \mathbf{a}^-_l\end{bmatrix} = \begin{bmatrix}\mathbf{B}^+ & \mathbf{B}^-\\ \mathbf{D}^+ & \mathbf{D}^-\end{bmatrix}\begin{bmatrix}\mathbf{a}^+_{l+1}\\ \mathbf{b}^-_{l+1}\end{bmatrix}. \tag{48}$$

The matrix entries are inner-products of Pridmore-Brown eigenfunctions and Bessel functions; for the matrices that correspond to the pressure equations we have

$$A^\pm_{\nu\mu} = (P^\pm_{l,\mu},\Psi_\nu) = \int_0^d P^\pm_{l,\mu}(r)\Psi_\nu(r)r\,\mathrm{d}r, \qquad B^\pm_{\nu\mu} = (P^\pm_{l+1,\mu},\Psi_\nu) = \int_0^d P^\pm_{l+1,\mu}(r)\Psi_\nu(r)r\,\mathrm{d}r. \tag{49}$$

The matrix entries of $\mathbf{C}^{\pm}$ and $\mathbf{D}^{\pm}$ corresponding to the axial velocity equations are computed analogously.

We consider the amplitudes of the waves propagating towards the interface as the unknowns. Rearranging leads to

$$\begin{matrix} & & \mu_{l+1} & \mu_l \\ {\scriptstyle \nu^{\max}} \\ {\scriptstyle \nu^{\max}} \end{matrix} \begin{bmatrix} \mathbf{B}^{+} & -\mathbf{A}^{-} \\ \mathbf{D}^{+} & -\mathbf{C}^{-} \end{bmatrix} \begin{bmatrix} \mathbf{a}_{l+1}^{+} \\ \mathbf{a}_{l}^{-} \end{bmatrix} = \begin{matrix} & & \mu_l & \mu_{l+1} \\ {\scriptstyle \nu^{\max}} \\ {\scriptstyle \nu^{\max}} \end{matrix} \begin{bmatrix} \mathbf{A}^{+} & -\mathbf{B}^{-} \\ \mathbf{C}^{+} & -\mathbf{D}^{-} \end{bmatrix} \begin{bmatrix} \mathbf{b}_{l}^{+} \\ \mathbf{b}_{l+1}^{-} \end{bmatrix}. \tag{50}$$

where the dimensions of the sub-matrices have been included. In this paper we restrict ourselves to locally reacting liners, so we choose $\mu_l = \mu^{\max}$, and choose $\nu^{\max} = \mu^{\max}$. Thus, we have $2\mu^{\max}$ equations and $\mu_l + \mu_{l+1} = 2\mu^{\max}$ unknowns. We remark that this approach can be extended to bulk absorbing liners, in which case the number of modes $\mu_l > \mu^{\max}$ (*i.e.* the number of degrees of freedom) depends on the depth of the liner, and consequently the system of equations needs to be extended with extra conditions [1, 9].

IV.B. Scattering Matrix Formalism

A naive coupling of the duct sections via the transmission and reflection matrices is possible, but this process is unstable in case of a large numbers of sections due to the exponentially decaying and increasing cut-off modes that are involved. An alternative approach would be an iterative one, where the propagation of a wave is only considered in the direction in which it decays. With this approach, the amplitudes are updated as more and more reflections and transmissions at different interfaces are taken into account at each new iteration, until the change in the amplitudes is below a certain threshold. However, this procedure may not converge for geometries with a large number of segments. We therefore follow the so-called "scattering matrix formalism" (see for example [14]), which has no convergence issues and is numerically stable.

We want to express the modal amplitude vectors of the outgoing waves in terms of the amplitude vectors of the incident waves. Thus, we write

$$\begin{bmatrix} \mathbf{a}_{l+1}^{+} \\ \mathbf{a}_{l}^{-} \end{bmatrix} = \begin{bmatrix} \mathbf{B}^{+} & -\mathbf{A}^{-} \\ \mathbf{D}^{+} & -\mathbf{C}^{-} \end{bmatrix}^{-1} \begin{bmatrix} \mathbf{A}^{+} & -\mathbf{B}^{-} \\ \mathbf{C}^{+} & -\mathbf{D}^{-} \end{bmatrix} \begin{bmatrix} \mathbf{b}_{l}^{+} \\ \mathbf{b}_{l+1}^{-} \end{bmatrix} = \begin{matrix} & \mu_l & \mu_{l+1} \\ {\scriptstyle \mu_{l+1}} \\ {\scriptstyle \mu_l} \end{matrix} \begin{bmatrix} \hat{\mathbf{S}}^{11} & \hat{\mathbf{S}}^{12} \\ \hat{\mathbf{S}}^{21} & \hat{\mathbf{S}}^{22} \end{bmatrix} \begin{bmatrix} \mathbf{b}_{l}^{+} \\ \mathbf{b}_{l+1}^{-} \end{bmatrix}, \tag{51}$$

where we introduced the *interface* scattering matrix $\hat{\mathbf{S}}$, including the sizes of the submatrices. Next, we want to combine the effect of scattering at the interface and propagation through the segment.

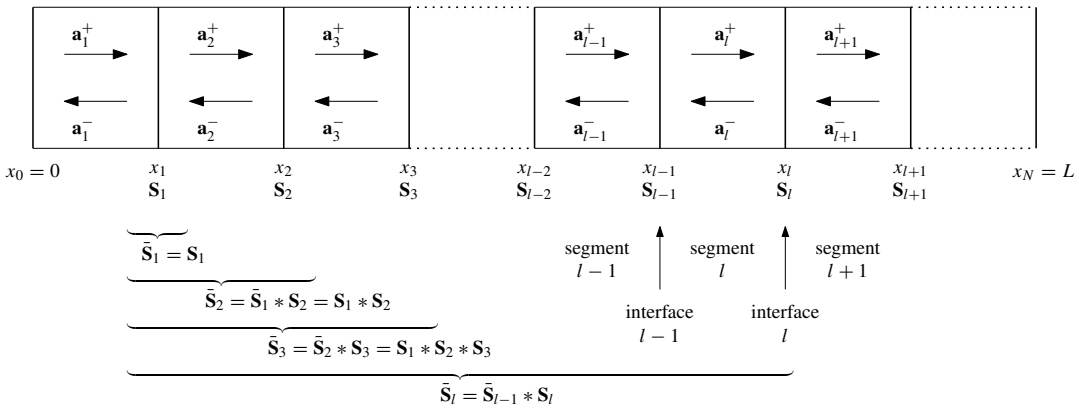

Figure 3. Schematic representation of the *S*-matrix algorithm.

Therefore, we introduce the *segment* scattering matrix $\mathbf{S}_l$ as follows:

$$\begin{bmatrix} \mathbf{a}_{l+1}^{+} \\ \mathbf{a}_{l}^{-} \end{bmatrix} = \begin{bmatrix} \hat{\mathbf{S}}_l^{11} & \hat{\mathbf{S}}_l^{12} \\ \hat{\mathbf{S}}_l^{21} & \hat{\mathbf{S}}_l^{22} \end{bmatrix} \begin{bmatrix} \mathbf{X}_l^{+} & 0 \\ 0 & \mathbf{X}_{l+1}^{-} \end{bmatrix} \begin{bmatrix} \mathbf{a}_{l}^{+} \\ \mathbf{a}_{l+1}^{-} \end{bmatrix} = \begin{bmatrix} \mathbf{S}_l^{11} & \mathbf{S}_l^{12} \\ \mathbf{S}_l^{21} & \mathbf{S}_l^{22} \end{bmatrix} \begin{bmatrix} \mathbf{a}_{l}^{+} \\ \mathbf{a}_{l+1}^{-} \end{bmatrix}. \tag{52}$$

where the propagation is accounted for by the diagonal matrices

$$(\mathbf{X}_l^+)_{\mu\mu} = \mathrm{e}^{\mathrm{i}k_{l,\mu}^+ h_l}, \quad (\mathbf{X}_{l+1}^-)_{\mu\mu} = \mathrm{e}^{-\mathrm{i}k_{l+1,\mu}^- h_{l+1}}, \quad h_l = x_l - x_{l-1}. \tag{53}$$

Note that the exponentials are always decaying.

The effect of all layers up to layer l can be combined in the *cumulative* scattering matrix $\bar{\mathbf{S}}_l$ (see also Figure 3):

$$\begin{bmatrix} \mathbf{a}_{l+1}^+ \\ \mathbf{a}_1^- \end{bmatrix} = \begin{bmatrix} \bar{\mathbf{S}}_l^{11} & \bar{\mathbf{S}}_l^{12} \\ \bar{\mathbf{S}}_l^{21} & \bar{\mathbf{S}}_l^{22} \end{bmatrix} \begin{bmatrix} \mathbf{a}_1^+ \\ \mathbf{a}_{l+1}^- \end{bmatrix}. \tag{54}$$

The cumulative scattering matrix of a certain set of segments can be computed by using the Redheffer star product, which is defined as

$$\begin{bmatrix} \mathbf{A}^{11} & \mathbf{A}^{12} \\ \mathbf{A}^{21} & \mathbf{A}^{22} \end{bmatrix} * \begin{bmatrix} \mathbf{B}^{11} & \mathbf{B}^{12} \\ \mathbf{B}^{21} & \mathbf{B}^{22} \end{bmatrix} = \begin{bmatrix} \mathbf{B}^{11}(\mathbf{I} - \mathbf{A}^{12}\mathbf{B}^{21})^{-1}\mathbf{A}^{11} & \mathbf{B}^{12} + \mathbf{B}^{11}\mathbf{A}^{12}(\mathbf{I} - \mathbf{B}^{21}\mathbf{A}^{12})^{-1}\mathbf{B}^{22} \\ \mathbf{A}^{21} + \mathbf{A}^{22}\mathbf{B}^{21}(\mathbf{I} - \mathbf{A}^{12}\mathbf{B}^{21})^{-1}\mathbf{A}^{11} & \mathbf{A}^{22}(\mathbf{I} - \mathbf{B}^{21}\mathbf{A}^{12})^{-1}\mathbf{B}^{22} \end{bmatrix}. \tag{55}$$

By using this definition $\bar{\mathbf{S}}_l$ can be computed as

$$\bar{\mathbf{S}}_l = \bar{\mathbf{S}}_{l-1} * \mathbf{S}_l = \mathbf{S}_1 * \cdots * \mathbf{S}_l. \tag{56}$$

The Redheffer star product can be constructed as as follows. We would like to construct the cumulative scattering matrix $\bar{\mathbf{S}}_l$ in order to compute the effect of segment l. Let us assume that we can describe the effect of all segments up to segment $l-1$ via

$$\begin{bmatrix} \mathbf{a}_l^+ \\ \mathbf{a}_1^- \end{bmatrix} = \begin{bmatrix} \bar{\mathbf{S}}_{l-1}^{11} & \bar{\mathbf{S}}_{l-1}^{12} \\ \bar{\mathbf{S}}_{l-1}^{21} & \bar{\mathbf{S}}_{l-1}^{22} \end{bmatrix} \begin{bmatrix} \mathbf{a}_1^+ \\ \mathbf{a}_l^- \end{bmatrix}. \tag{57}$$

Furthermore, we have at interface l:

$$\begin{bmatrix} \mathbf{a}_{l+1}^+ \\ \mathbf{a}_l^- \end{bmatrix} = \begin{bmatrix} \mathbf{S}_l^{11} & \mathbf{S}_l^{12} \\ \mathbf{S}_l^{21} & \mathbf{S}_l^{22} \end{bmatrix} \begin{bmatrix} \mathbf{a}_l^+ \\ \mathbf{a}_{l+1}^- \end{bmatrix}. \tag{58}$$

Substitute the second row of (58) into the first row of (57) to obtain

$$\mathbf{a}_l^+ = \bar{\mathbf{S}}_{l-1}^{11}\mathbf{a}_1^+ + \bar{\mathbf{S}}_{l-1}^{12}\mathbf{a}_l^- = \bar{\mathbf{S}}_{l-1}^{11}\mathbf{a}_1^+ + \bar{\mathbf{S}}_{l-1}^{12}\left[\mathbf{S}_l^{21}\mathbf{a}_l^+ + \mathbf{S}_l^{22}\mathbf{a}_{l+1}^-\right]. \tag{59}$$

Collecting the terms gives

$$\left[\mathbf{I} - \bar{\mathbf{S}}_{l-1}^{12}\mathbf{S}_l^{21}\right]\mathbf{a}_l^+ = \bar{\mathbf{S}}_{l-1}^{11}\mathbf{a}_1^+ + \bar{\mathbf{S}}_{l-1}^{12}\mathbf{S}_l^{22}\mathbf{a}_{l+1}^-, \tag{60}$$

so

$$\mathbf{a}_l^+ = \left[\mathbf{I} - \bar{\mathbf{S}}_{l-1}^{12}\mathbf{S}_l^{21}\right]^{-1}\bar{\mathbf{S}}_{l-1}^{11}\mathbf{a}_1^+ + \left[\mathbf{I} - \bar{\mathbf{S}}_{l-1}^{12}\mathbf{S}_l^{21}\right]^{-1}\bar{\mathbf{S}}_{l-1}^{12}\mathbf{S}_l^{22}\mathbf{a}_{l+1}^-. \tag{61}$$

Substituting this into the first row of (58) yields

$$\mathbf{a}_{l+1}^+ = \overbrace{\mathbf{S}_l^{11}\left[\mathbf{I} - \bar{\mathbf{S}}_{l-1}^{12}\mathbf{S}_l^{21}\right]^{-1}\bar{\mathbf{S}}_{l-1}^{11}}^{\bar{\mathbf{S}}_l^{11}}\mathbf{a}_1^+ + \underbrace{\left\{\mathbf{S}_l^{11}\left[\mathbf{I} - \bar{\mathbf{S}}_{l-1}^{12}\mathbf{S}_l^{21}\right]^{-1}\bar{\mathbf{S}}_{l-1}^{12}\mathbf{S}_l^{22} + \mathbf{S}_l^{12}\right\}}_{\bar{\mathbf{S}}_l^{12}}\mathbf{a}_{l+1}^-. \tag{62}$$

Analogously, we can substitute the first row of (57) into the second row of (58) to obtain

$$\left[\mathbf{I} - \mathbf{S}_l^{21}\bar{\mathbf{S}}_{l-1}^{12}\right]\mathbf{a}_l^- = \mathbf{S}_l^{21}\bar{\mathbf{S}}_{l-1}^{11}\mathbf{a}_1^+ + \mathbf{S}_l^{22}\mathbf{a}_{l+1}^-, \tag{63}$$

from which follows

$$\mathbf{a}_l^- = \left[\mathbf{I} - \mathbf{S}_l^{21}\bar{\mathbf{S}}_{l-1}^{12}\right]^{-1}\mathbf{S}_l^{21}\bar{\mathbf{S}}_{l-1}^{11}\mathbf{a}_1^+ + \left[\mathbf{I} - \mathbf{S}_l^{21}\bar{\mathbf{S}}_{l-1}^{12}\right]^{-1}\mathbf{S}_l^{22}\mathbf{a}_{l+1}^-. \tag{64}$$

Substituting this into the second row of (57) yields

$$\mathbf{a}_1^- = \overbrace{\left\{\bar{\mathbf{S}}_{l-1}^{21} + \bar{\mathbf{S}}_{l-1}^{22}\left[\mathbf{I} - \mathbf{S}_l^{21}\bar{\mathbf{S}}_{l-1}^{12}\right]^{-1}\mathbf{S}_l^{21}\bar{\mathbf{S}}_{l-1}^{11}\right\}}^{\bar{\mathbf{s}}_l^1}\mathbf{a}_1^+ + \underbrace{\bar{\mathbf{S}}_{l-1}^{22}\left[\mathbf{I} - \mathbf{S}_l^{21}\bar{\mathbf{S}}_{l-1}^{12}\right]^{-1}\mathbf{S}_l^{22}}_{\bar{\mathbf{s}}_l^{12}}\mathbf{a}_{l+1}^-. \tag{65}$$

These equations can still be used when the number of modes is different for each segment (*i.e.* when the four blocks of the scattering matrices are not square). To see this, consider the total number of amplitudes for the three segments numbered 1, l and $l+1$, which is $2\mu_1 + 2\mu_l + 2\mu_{l+1}$. Of these amplitudes the $\mu_1 + \mu_{l+1}$ amplitudes of the incident waves in segments 1 and $l+1$ are known. Hence, the other amplitudes can be determined by using the $\mu_1 + 2\mu_l + \mu_{l+1}$ equations of (57) and (58). Also note that the dimensions of the terms between square brackets in (62) and (65) are $\mu_l \times \mu_l$, so only the solution of square systems is required.

Consequently, if all of the segment scattering matrices and the incoming amplitudes $\mathbf{a}_1^+$ and $\mathbf{a}_N^-$ of the outer segments are known, then the outgoing amplitudes and hence the total field in the outer segments can be computed. To compute the field inside the entire duct the amplitudes in intermediate segments are required as well. We compute these by using (59) and the second row of (58). Note that we did not invert the propagation matrices $\mathbf{X}_l$, which would have caused growing exponentials (which might provoke numerical problems).

IV.C. Matching Conditions Based on the Bilinear Map

In this section we set up a system of equations which has the same structure as (48) for the classical mode-matching approach.

Let us define the vector $\hat{\boldsymbol{f}}$ whose components are the acoustic pressure and the velocity components:

$$\hat{\boldsymbol{f}}_l(x,r) = \left[p_l(x,r), \hat{u}_l(x,r), \hat{v}_l(x,r), \hat{w}_l(x,r)\right]. \tag{66}$$

The total field for a given circumferential wavenumber m in each segment is a superposition of all modes:

$$\hat{\boldsymbol{f}}_l(x,r) = \sum_{\mu=1}^{\infty}\Big(a_{l,\mu}^+\boldsymbol{F}_{l,\mu}^+(r)\,\mathrm{e}^{\mathrm{i}k_{l,\mu}^+(x-x_{l-1})} + a_{l,\mu}^-\boldsymbol{F}_{l,\mu}^-(r)\,\mathrm{e}^{\mathrm{i}k_{l,\mu}^-(x-x_l)}\Big), \quad x_{l-1} \leqslant x \leqslant x_l, \tag{67}$$

where $\boldsymbol{F}$ again denotes the vector of perturbation amplitudes. At the interface at $x = x_l$ we have

$$\hat{\boldsymbol{f}}_l(r) = \sum_{\mu=1}^{\mu_l}\Big(b_{l,\mu}^+\boldsymbol{F}_{l,\mu}^+(r) + a_{l,\mu}^-\boldsymbol{F}_{l,\mu}^-(r)\Big), \tag{68}$$

$$\hat{\boldsymbol{f}}_{l+1}(r) = \sum_{\mu=1}^{\mu_{l+1}}\Big(a_{l+1,\mu}^+\boldsymbol{F}_{l+1,\mu}^+(r) + b_{l+1,\mu}^-\boldsymbol{F}_{l+1,\mu}^-(r)\Big). \tag{69}$$

Inside the duct we impose continuity of $p(x,r)$, $u(x,r)$, $v(x,r)$ and $w(x,r)$ by applying the bilinear form to $\hat{\boldsymbol{f}}_l = \hat{\boldsymbol{f}}_{l+1}$ with the solution of the associated problem $\boldsymbol{\Psi}_\nu$, which results in

$$\sum_{\mu=1}^{\mu_l} b_{l,\mu}^+\langle\boldsymbol{F}_{l,\mu}^+, \boldsymbol{\Psi}_\nu\rangle + a_{l,\mu}^-\langle\boldsymbol{F}_{l,\mu}^-, \boldsymbol{\Psi}_\nu\rangle = \sum_{\mu=1}^{\mu_{l+1}} a_{l+1,\mu}^+\langle\boldsymbol{F}_{l+1,\mu}^+, \boldsymbol{\Psi}_\nu\rangle + b_{l+1,\mu}^-\langle\boldsymbol{F}_{l+1,\mu}^-, \boldsymbol{\Psi}_\nu\rangle, \tag{70}$$

for $\nu = -\nu^{\max}, \ldots, -1, 1, \ldots, \nu^{\max}$. When we split the range of ν into left ($\nu < 0$) and right ($\nu > 0$) running parts, we again obtain in matrix format

$$\begin{bmatrix}\mathbf{A}^+ & \mathbf{A}^-\\ \mathbf{C}^+ & \mathbf{C}^-\end{bmatrix}\begin{bmatrix}\mathbf{b}_l^+\\ \mathbf{a}_l^-\end{bmatrix} = \begin{bmatrix}\mathbf{B}^+ & \mathbf{B}^-\\ \mathbf{D}^+ & \mathbf{D}^-\end{bmatrix}\begin{bmatrix}\mathbf{a}_{l+1}^+\\ \mathbf{b}_{l+1}^-\end{bmatrix}. \tag{71}$$

In order to prevent unnecessary computation of an extra set of eigenfunctions, we can choose as test function $\boldsymbol{\Psi}_\nu$ the eigensolutions of, say, segment l. In that case the matrix entries can be computed as

$$\{A, C\}^{\pm}_{\nu\mu} = \langle \boldsymbol{F}_{l\mu}, \boldsymbol{F}_{l\nu} \rangle, \tag{72a}$$

$$\{B, D\}^{\pm}_{\nu\mu} = \langle \boldsymbol{F}_{l+1,\mu}, \boldsymbol{F}_{l\nu} \rangle, \tag{72b}$$

where

$$\{A, B\}^{+} : \mu > 0, \nu > 0, \qquad \{C, D\}^{+} : \mu > 0, \nu < 0,$$
$$\{A, B\}^{-} : \mu < 0, \nu > 0, \qquad \{C, D\}^{-} : \mu < 0, \nu < 0.$$

The values of the bilinear forms in (72) can be computed as follows. Suppose that we know the set of eigensolutions for two segments l and n, with possibly different liner properties. When $Z_l \neq Z_n$ then the sets of axial wavenumbers have in general (except for a rare coincidence) no values in common, so it holds that $k_{l\mu} \neq k_{n\nu}$. Consequently we can use (39) to compute

$$\langle \boldsymbol{F}_{l\mu}, \boldsymbol{F}_{n\nu} \rangle = \frac{\mathrm{i}d P_{l\mu} P_{n\nu}}{\Omega_{n\nu}\omega(k_{l\mu} - k_{n\nu})} \left[\frac{\Omega_{l\mu}}{Z_{l\mu}} - \frac{\Omega_{n\nu}}{Z_{n\nu}} \right]\Bigg|_{r=d}, \qquad \text{for} \quad Z_l \neq Z_n. \tag{73}$$

For the case when $Z_l = Z_n := Z$ we can have $\mu \neq \nu$, which means that $k_{l\mu} \neq k_{n\nu}$, so we can compute

$$\langle \boldsymbol{F}_{l\mu}, \boldsymbol{F}_{n\nu} \rangle = -\frac{\mathrm{i}d P_{l\mu} P_{n\nu} u_0}{\Omega_{n\nu}\omega Z}\Bigg|_{r=d}, \qquad \text{for} \quad Z_l = Z_n, \quad \mu \neq \nu, \tag{74}$$

which is identically zero for non-slipping flow ($u_0(d) = 0$) or a hard wall ($Z \to \infty$). When $\mu = \nu$ we have $k_{l\mu} = k_{n\nu} := k_\mu$ and $P_{l\mu} = P_{n\nu} := P_\mu$. We require the solution $\hat{P}_\mu$ of the inhomogeneous Pridmore-Brown equation (41) to compute

$$\langle \boldsymbol{F}_{l\mu}, \boldsymbol{F}_{n\nu} \rangle = \frac{d}{\rho_0 \Omega_\mu^2} \left[\hat{P}_\mu P'_\mu - \frac{u_0}{\Omega_\mu} P'_\mu P_\mu - \hat{P}'_\mu P_\mu \right]_{r=d}, \qquad \text{for} \quad Z_l = Z_n, \quad \mu = \nu. \tag{75}$$

Note that this implies that $\mathbf{A}^+$ and $\mathbf{C}^-$ are diagonal matrices, and $\mathbf{A}^-$ and $\mathbf{C}^+$ zero matrices for non-slipping flow or hard wall.

V. Numerical Results

In order to compare the results of the classical (CMM) and the bilinear-map-based (BLM) mode-matching approaches, we consider the test cases which are listed in Table 1. The 1m long duct with radius 0.15m is split into two segments at x = 0.5m (except for configuration IV); the left segment has a hard wall, and the right hand side segment has a locally reacting impedance wall. The incident field consists of one right-running mode, either $\mu = 1$ or 2 for the pertinent configurations[5]. For the BLM-based results the modes of the left (hard-wall) segment are used as test functions.

The results in this section are made dimensionless by scaling on the duct radius d, a reference density ρ_∞ and a reference temperature T_∞. This implies that velocities are scaled on reference sound speed $c_\infty = \sqrt{\gamma \mathcal{R} T_\infty}$ and time on d/c_∞. The non-dimensional mean flow axial velocity is denoted by M (the Mach number), *i.e.* $u_0 = c_\infty M$.

Configuration II has a slipping flow, hence it is necessary to use the Ingard-Myers boundary condition here, this in contrast to configurations I and III which have non-slipping flow. The mean flow profile for configuration II has the equivalent mass flow as a uniform flow with Mach number 0.3. The non-uniform temperature profile of configuration III has the equivalent mass flow of a constant mean temperature of $T = 1$. The flow profile of configuration III is more representative of a uniform flow with a thin boundary layer. Configuration IV is a duct with $N = 20$ segments, where the impedances of the segments have an imaginary part that varies linearly between -3 and 3. For all configurations we use $\mu^{\max} = 50$ modes to represent the field.

Configuration	I	II	III	IV
Helmholtz & azi.	$\omega = 13.86, m = 5$	$\omega = 8.86, m = 5$	$\omega = 15, m = 5$	$\omega = 15, m = 5$
Temperature	$T = 1$	$T = 1$	$T = 2\log(2)(1 - \frac{r^2}{2})$	$T = 1$
Mean flow	$M = 0.5(1 - r^2)$	$M = 0.3 \cdot \frac{4}{3}(1 - \frac{r^2}{2})$	$M = 0.3 \cdot \tanh(10(1 - r))$	$M = 0.3 \cdot \tanh(10(1 - r))$
Soft-wall impedance	$Z = 1 - 1i$	$Z = 1 + 1i$	$Z = 1 - 1i$	$Z = 1 - 3i, \ldots, 1 + 3i,$ $N = 20$
Incident rad. mode nr.	$\mu = 1$	$\mu = 1$	$\mu = 2$	$\mu = 1$

Table 1. Test configurations. $\mu^{\max} = 50$ for all configurations.

To compute the solutions of the boundary value problems we use a path-following approach as described in [15]. Both for locally and non-locally reacting liners we start the path-following process from the solutions for a uniform flow and constant temperature. Subsequently the liner and flow properties are gradually changed to the target configuration.

Finding the uniform-flow constant-temperature solutions amounts to finding the complex-valued roots of an analytic function. To compute these roots we employ the method of Delves and Lyness [16]. This method first constructs a polynomial that has the same roots as the analytic function of interest by using contour integration (*i.e.* numerical quadrature). Subsequently the roots of the polynomial can be computed in a standard manner. The advantage of this method lies in the fact that it is guaranteed that all roots inside a given area are found (apart from finite numerical accuracy issues), whereas a Newton method only converges to all of the roots if it is started from sufficiently close initial guesses. The location of these initial guesses for the Newton method is not always self-evident, as for example in case of surface waves [17]. Figure 4 shows an example of the paths of the axial wavenumbers for the first configuration.

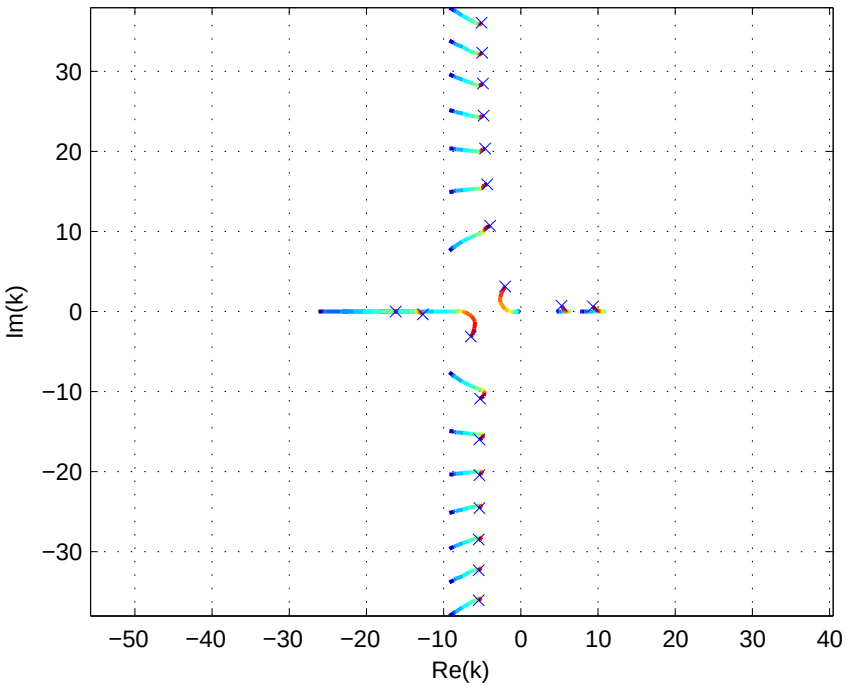

Figure 4. Axial wavenumber paths for configuration I, first 10 modes in both directions, moving from blue to red, 'x' is the final wavenumber belonging to the right-hand side (soft-wall) segment.

It is, moreover, important to note that it is not necessary to use path-following for the inhomogeneous problem, since the axial wave number k_μ is given and not part of the solution, and the inhomogeneous problem (with inhomogeneous boundary condition at $r = d$) has a unique solution. Consequently, it is

[5]For non-uniform flow and/or temperature the numbering of the modes is not unambiguous; we number them according their similarity in eigenfunction shape and axial wavenumber value to the uniform flow modes.

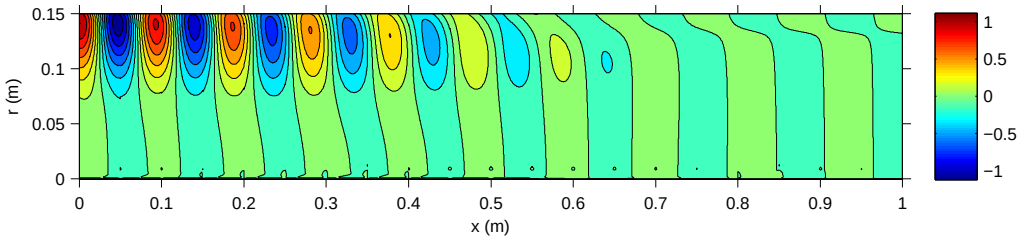

Figure 5. Real part of pressure field for configuration IV.

much cheaper to solve the inhomogeneous problem than the original eigenvalue problem.

To illustrate that a high number of segments poses no problem for mode-matching with the scattering matrix formalism we included Figure 5, which depicts the pressure field for a configuration with $N = 20$ segments. From our experience, an iterative procedure often does not converge for more than 10 segments. The artifacts near $r = 0$ are due to the fact that the field there is almost zero, very close to the level curve at zero.

Figure 6 shows the acoustic pressure field for both the classical (CMM) and the bilinear form (BLM) based mode-matching approaches for configuration I. Figures 7, 8 and 9 compare the pressure, axial and radial velocity for both mode-matching methods at several radial locations. As can be seen, the results of the two approaches are in very good agreement for all configuration I-III.

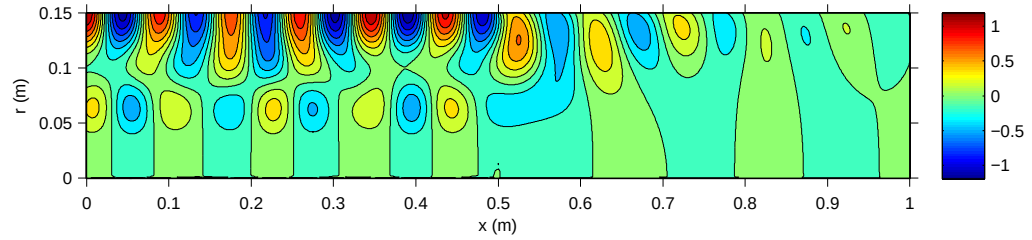

(a) Classical mode-matching.

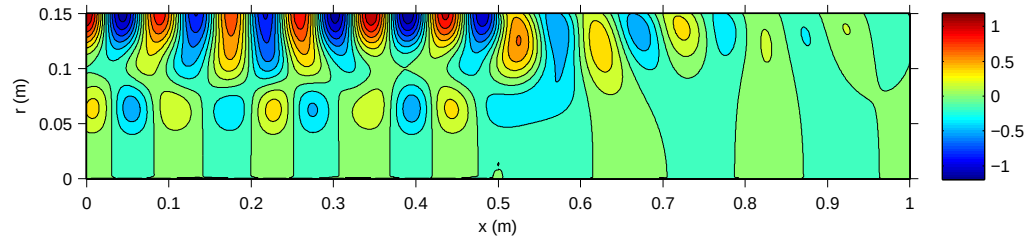

(b) Bilinear map-based mode-matching.

Figure 6. Real part of pressure field for configuration I.

The validity of the numerical results can be assessed by checking whether they satisfy the balance of energy. For that purpose we use the exact Myers' Energy Corollary (see Appendix A). Figure 10 shows the sum of the acoustic fluxes through the wall, the inlet and the outlet plane, and the volume integral over the source term. We use a relative numerical accuracy of 10^{-6} for the boundary value problem solver, and use Simpson's rule for the numerical quadrature on a grid of 151 by 1001 grid points. Thus, this sum (which is normalized on the flux through the inlet plane), which ideally should be zero, is not expected to be bigger than 10^{-6}. Figure 10 shows that the energy balance is satisfied better as the number of modes $\mu^{\max}$ increases, which is to be expected. Furthermore, the bilinear-form based mode-matching method performs even better than the classical one for this configuration I. Incidentally, the energy integral being so accurately satisfied confirms the assumption of a negligible continuous spectrum contribution.

In order to verify the regular behavior of the solution at the hard-soft singularities along the wall

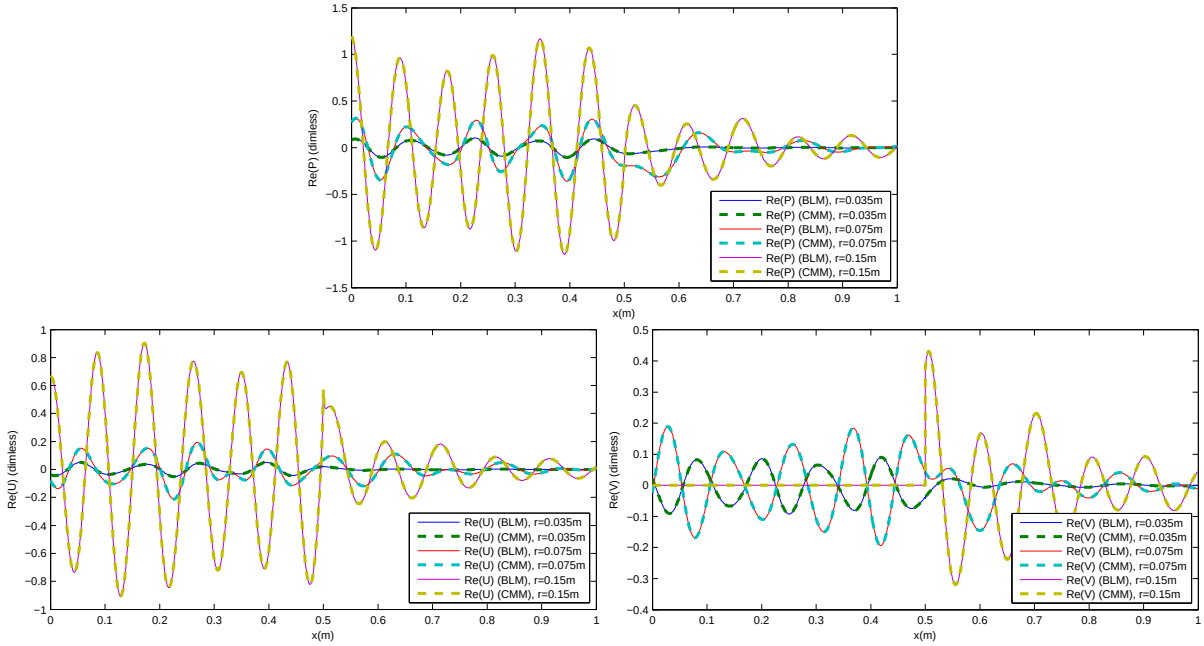

Figure 7. Comparison of classical (CMM) and bilinear-map-based (BLM) mode-matching approaches for configuration I. Pressure, axial and radial velocity at radial locations: $r = \{0.035, 0.075, 0.15\}$ m**.**

(where a so-called edge condition [18, 19] has to be satisfied, which is that any volume surrounding the edge carries finite energy) we check the uniform convergence of the modal series via the convergence rate of the found amplitudes A_n.

If we assume that $A_n = O(n^p)$ for $n \to \infty$ such that $\log |A_n| = p \log n + O(1)$, then for p_n defined by

$$p_n = \frac{\log |A_n|}{\log n} \tag{76}$$

p_n is expected to approach p with $p_n = p + O(1/\log(n))$.

Anticipating a local behavior of the modal functions that is asymptotically similar to a Fourier series, a convergence rate $p < -1$ will be sufficient for uniform convergence. For the configurations considered, with $p \simeq -2$, we see that this is indeed the case, in particular for both mode matching methods in the same way, see Figure 11.

Moreover, there is another interesting observation possible from these plots. The behavior of p_n from the classical matching method is not as smooth as from the bilinear-map-based matching as n becomes larger. Apparently, the amplitudes from the classical method are more inaccurate for large n. This is an interesting confirmation of the fact that the inner-products based on exact relations are not prone to the oscillation quadrature errors for large n.

VI. Conclusion

Mode matching is a particularly successful method for problems of time harmonic wave propagation in ducts of circular or rectangular cross section, with a uniform medium. The simple geometry and the simple medium properties result in just Besselfunctions, or cosine and sine functions, respectively, for the modal shape functions. For these functions the standard L_2 integral inner-products can be expressed in closed form, and the elements of the mode matching matrices can be determined analytically exactly, leaving the mode matching problem as a relatively easy linear algebra problem, that can be solved fast and accurately.

All these advantages disappear for ducts with a (cross-wise) non-uniform medium. Modes, *i.e.* solutions of the form $\sim f(y, z)\, \mathrm{e}^{\mathrm{i}kx}$, still exist, but their mode shape is not simple anymore, and certainly integrals of their products are not available in closed form. As a result, the method of mode matching will

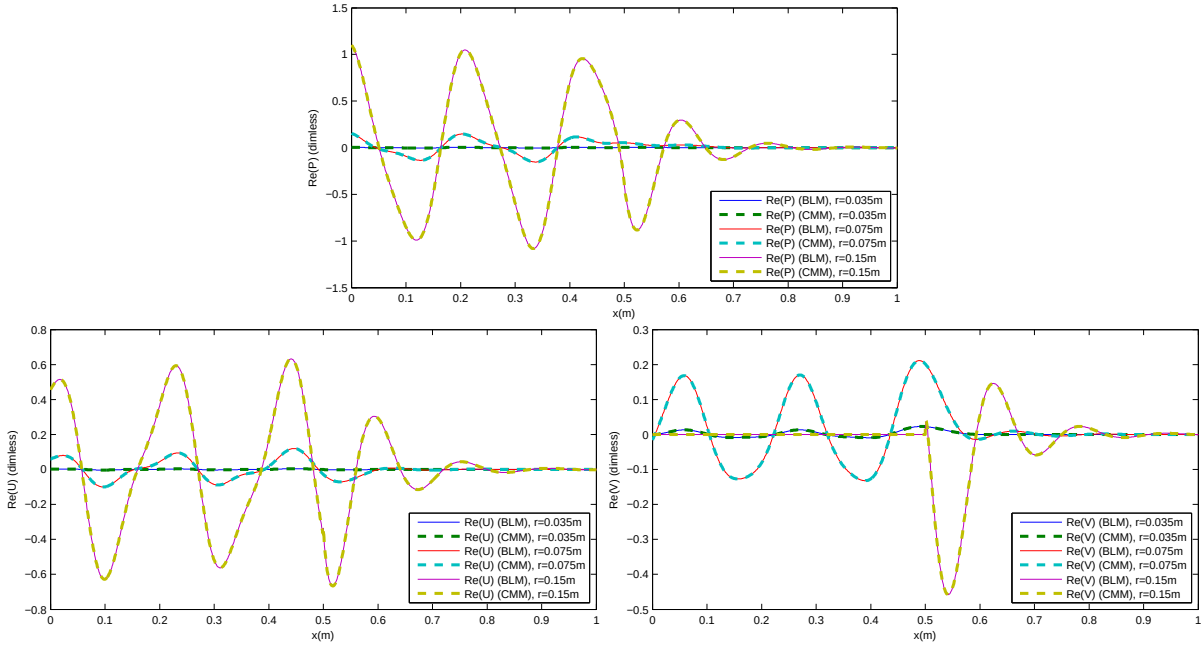

Figure 8. Comparison of classical (CMM) and bilinear-map-based (BLM) mode-matching approaches for configuration II. Pressure, axial and radial velocity at radial locations: $r = \{0.035, 0.075, 0.15\}$ m**.**

require a large amount of numerical quadrature, on top of the numerical exercise necessary to determine the mode shape functions. Since the modal shape functions will show increasingly oscillatory behaviour with increasing modal order, the integrals for the highest orders will inherently be prone to numerical error and difficult, or at least expensive, to determine.

The method, presented in this paper, avoids these problems by constructing an alternative "inner-product", such that, when applied to modal shape functions, they are explicitly available in closed form (for the radially symmetric problem) or simplify to a line integral along the boundary (in the general 2D problem). Although the proposed "inner-product" is not a real inner-product, which is why we call it here a bilinear form, the behaviour in the mode matching method is entirely the same as for the inner-product in the classical approach. By their construction, the present integrals can be considered as the natural generalisations of the Besselfunction product integrals.

In order to make a start with establishing a firm mathematical basis for the method, we compared the new method with an implementation of the classical method with hard-wall radial modes (Bessel-functions) as test functions, known to form a complete basis. The results are in full agreement with each other, while the anticipated efficiency and accuracy is indeed realised.

Although the elegance is very appealing, a lot of research is to be done, both numerically and functional analytically, as we have explored only a fraction of the mathematical ramifications yet.

Acknowledgments

We gratefully acknowledge the fruitful discussions with Professor R.M.M. Mattheij of the Mathematics Department at Eindhoven University of Technology, and particularly appreciate his insights and guidance in matters of numerical analysis.

A. Myers' Energy Corollary

When the equations for conservation of mass and momentum and the general energy conservation law for fluid motion are expanded to quadratic order, this 2nd order energy term may be reduced to the

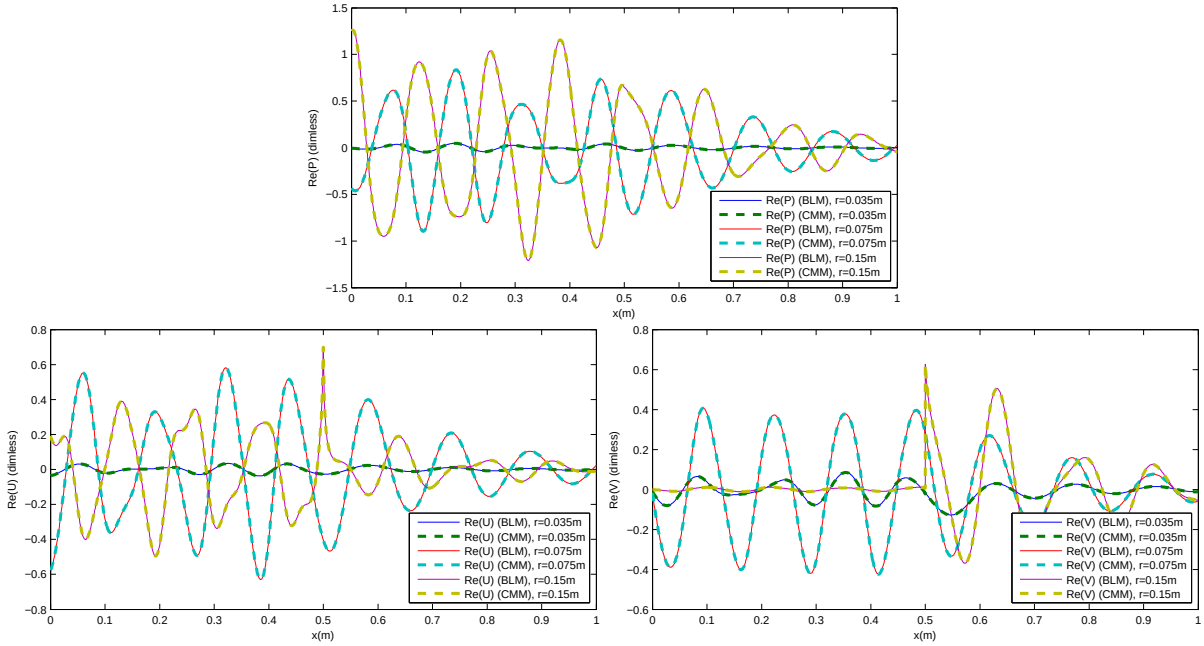

Figure 9. Comparison of classical (CMM) and bilinear-map-based (BLM) mode-matching approaches for configuration III. Pressure, axial and radial velocity at radial locations: $r = \{0.035, 0.075, 0.15\}$ m**.**

following conservation law for perturbation energy density E, energy flux $\boldsymbol{I}$, and dissipation $\mathcal{D}$

$$\frac{\partial E}{\partial t} + \nabla \cdot \boldsymbol{I} = -\mathcal{D} \tag{77}$$

with

$$E = \frac{p_1^2}{2\rho_0 c_0^2} + \frac{1}{2}\rho_0 |\boldsymbol{v}_1|^2 + \rho_1 \boldsymbol{v}_0 \cdot \boldsymbol{v}_1 + \frac{\rho_0 T_0 s_1^2}{2C_p}, \tag{78a}$$

$$\boldsymbol{I} = (\rho_0 \boldsymbol{v}_1 + \rho_1 \boldsymbol{v}_0)\left(\frac{p_1}{\rho_0} + \boldsymbol{v}_0 \cdot \boldsymbol{v}_1\right) + \rho_0 \boldsymbol{v}_0 T_1 s_1, \tag{78b}$$

$$\mathcal{D} = -\rho_0 \boldsymbol{v}_0 \cdot (\boldsymbol{\omega}_1 \times \boldsymbol{v}_1) - \rho_1 \boldsymbol{v}_1 \cdot (\boldsymbol{\omega}_0 \times \boldsymbol{v}_0) + s_1(\rho_0 \boldsymbol{v}_1 + \rho_1 \boldsymbol{v}_0) \cdot \nabla T_0 - s_1 \rho_0 \boldsymbol{v}_0 \cdot \nabla T_1, \tag{78c}$$

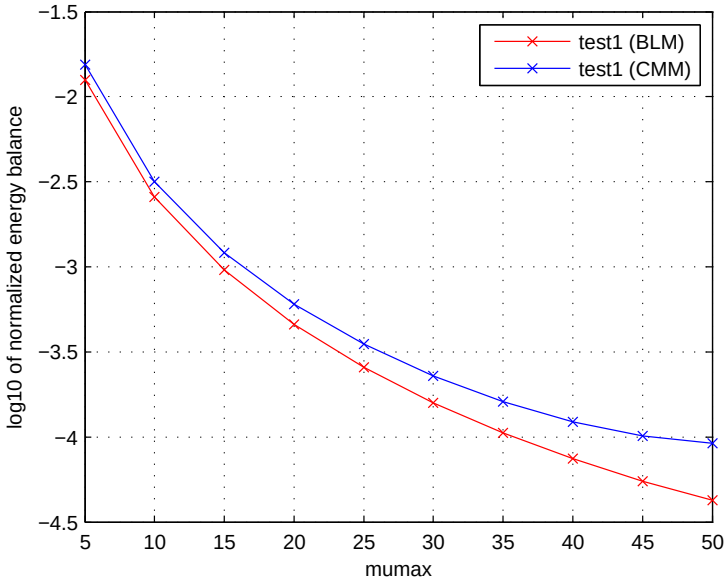

Figure 10. Comparison of classical (CMM) and bilinear-map-based (BLM) mode-matching approaches for configuration I. Energy balance (normalized on flux through inlet plane) versus $\mu^{\max}$**.**

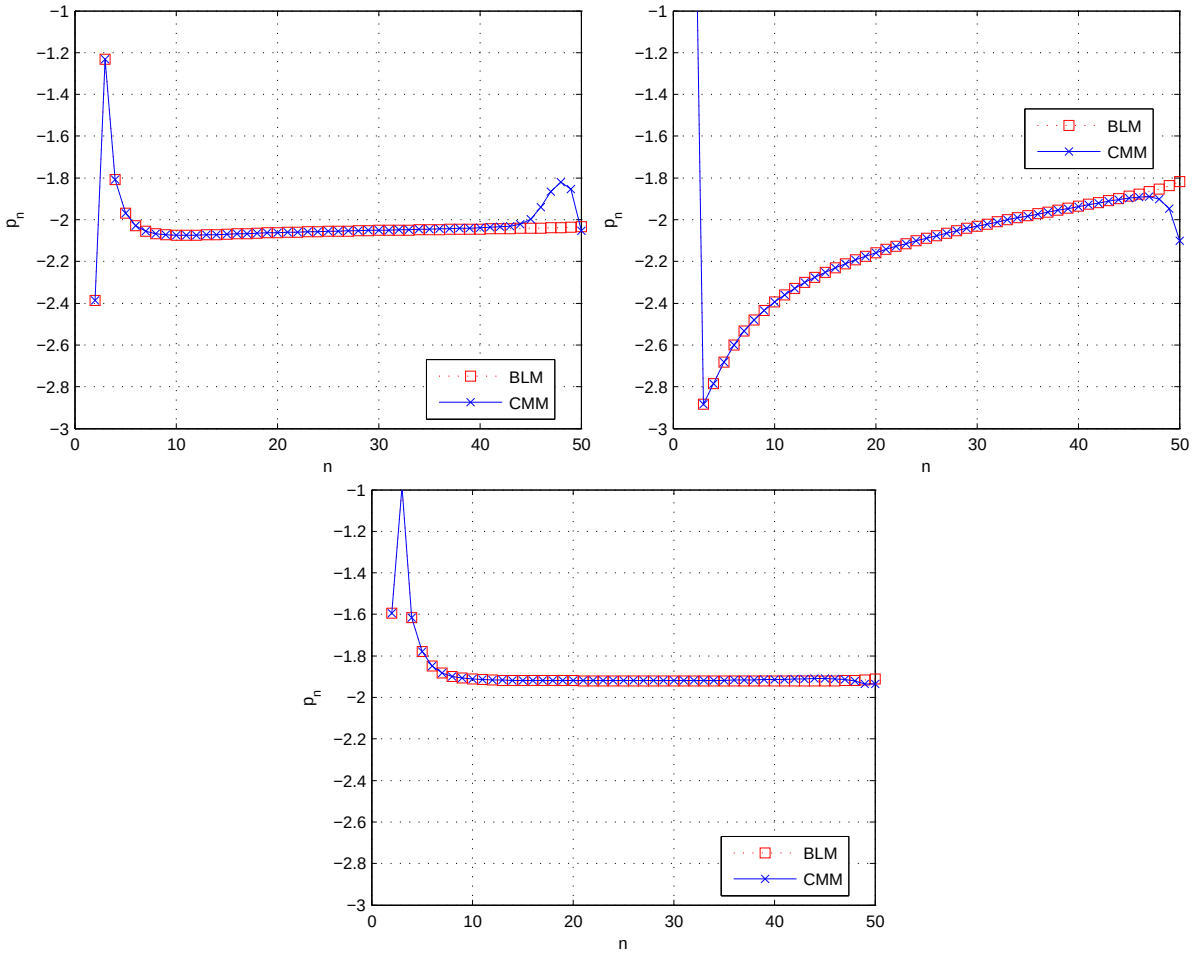

Figure 11. Convergence rate of amplitudes for classical and bilinear-map-based mode-matching, for configurations I, II and III.

as shown by Myers [20]. The vorticity here is denoted by $\boldsymbol{\omega} = \nabla \times \boldsymbol{v}$. Note that these equations only contain zeroth and first order terms. Consequently, this conservation law is exactly valid for small linear disturbances (p_1, $\boldsymbol{v}_1$, etc.) of a mean flow (p_0, $\boldsymbol{v}_0$, etc.) which can have non-uniform velocity and temperature. Taking the time average of (77) for time harmonic perturbations yields

$$\nabla \cdot \overline{\boldsymbol{I}} = -\overline{\mathcal{D}}. \tag{79}$$

By taking the volume integral of (79) over a volume $\mathcal{V}$ with boundary $\partial\mathcal{V}$ and applying the divergence theorem, we find

$$\int_{\partial\mathcal{V}} \overline{\boldsymbol{I}} \cdot \boldsymbol{n} \, \mathrm{d}A + \int_{\mathcal{V}} \overline{\mathcal{D}} \, \mathrm{d}V = 0. \tag{80}$$

References

[1]Nodé-Langlois, T., Sijtsma, P., Moal, S., and Vieuille, F., "Modelling of Non-Locally Reacting Acoustic Treatments for Aircraft Ramp Noise Reduction," *16th AIAA/CEAS Aeroacoustics Conference, Stockholm, Sweden*, No. AIAA 2010-3769, June 7-9 2010.

[2]Astley, R., Hii, V., and Gabard, G., "A computational mode-matching aproach for propagation in three-dimensional ducts with flow," *12th AIAA/CEAS Aeroacoustics Conference, Cambridge(MA), USA*, No. AIAA 2006-2528, May 8-10 2006.

[3]Watson, G. N., *A Treatise on the Theory of Bessel Functions*, Cambridge University Press, 1995.

[4]Rienstra, S. W. and Darau, M., "Boundary Layer Thickness Effects of the Hydrodynamic Instability along an Impedance Wall," *J. Fluid Mech.*, Vol. 671, 2011, pp. 559–573.

[5]Brambley, E. J., Darau, M., and Rienstra, S. W., "The critical layer in linear-shear boundary layers over acoustic linings," *J. Fluid Mech.*, Vol. 710, 2012, pp. 545–568.

[6]Goldstein, M. E., *Aeroacoustics*, McGraw-Hill International Book Co., New York, 1976.

[7]Rienstra, S. W. and Hirschberg, A., "An Introduction to Acoustics," Tech. Rep. IWDE 92-06, Technische Universiteit Eindhoven, 1992-2004-2011, http://www.win.tue.nl/∼sjoerdr/papers/boek.pdf.

[8]Pridmore-Brown, D., "Sound propagation in a fluid flowing through an attenuating duct," *J. Fluid Mech.*, Vol. 4, 1958, pp. 393–406.

[9]Sijtsma, P. and van der Wal, H., "Modelling a Spiralling Type of Non-Locally Reacting Liner," *9th AIAA/CEAS Aeroacoustics Conference and Exhibit, Hilton Head, South Carolina*, No. AIAA 2003-3308, 2003.

[10]Myers, M. K., "On the acoustic boundary condition in the presence of flow," *J. Sound Vib.*, Vol. 71, 1980, pp. 429–434.

[11]Kreyszig, E., *Introductory Functional Analysis with Applications*, John Wiley & Sons, Wiley Classics Library ed., 1989.

[12]Sofrin, T. and Cicon, D., "Ducted fan noise propagation in non-uniform flow. II-Wave equation solution," *AIAA 11th Aeroacoustics Conference, Palo Alto (CA), USA*, No. AIAA 87-2702, October 19-21 1987.

[13]Cooper, A. J. and Peake, N., "Propagation of unsteady disturbances in a slowly varying duct with mean swirling flow," *J. Fluid Mech.*, Vol. 445, 2001, pp. 207–234.

[14]Li, L., "Formulation and comparison of two recursive matrix algorithms for modeling layered diffraction gratings," *J. Opt. Soc. Am. A*, Vol. 13, No. 5, May 1996, pp. 1024–1035.

[15]Oppeneer, M., Lazeroms, W. M., Rienstra, S. W., Sijtsma, P., and Mattheij, R. M., "Acoustic modes in a duct with slowly varying impedance and non-uniform mean flow and temperature," *17th AIAA/CEAS Aeroacoustics Conference, Portland(OR), USA*, No. AIAA 2011-2871, June 5-8 2011.

[16]Delves, L. and Lyness, J., "A numerical method for locating the zeros of an analytic function," *Math. Comp.*, Vol. 21, 1966, pp. 543–560.

[17]Rienstra, S. W., "A classification of duct modes based on surface waves," *Wave Motion*, Vol. 37, No. 2, 2003, pp. 119–135.

[18]Jones, D. S., *The Theory of Electromagnetism*, Pergamon Press, 1964, pp. 566–569.

[19]Mittra, R., Itoh, T., and Li, T.-S., "Analytical and numerical studies of the relative convergence phenomenon arising in the solution of an integral equation by the moment method," *IEEE Transactions on Microwave Theory and Techniques*, Vol. 20, No. 2, 1972, pp. 96–104.

[20]Myers, M. K., "Transport of energy by disturbances in arbitrary steady flows," *Journal of Fluid Mechanics*, Vol. 226, 1991, pp. 383–400.